INTERNATIONAL JOURNAL OF PRECISION ENGINEERING AND MANUFACTURING Vol. 15, No. 8, pp. 1513-1519 AUGUST 2014 / 1513
DOI: 10.1007/s12541-014-0499-2

Tip Shape Effect on Hot Nanoindentation Hardness and Modulus Measurements

Miguel Alberto Monclús[1,#], Saeid Lotfian[1], and Jon Mikel Molina-Aldareguía[1]

1 IMDEA Materials Institute, C/Eric Kandel 2, 28906, Getafe, Madrid, Spain
Corresponding Author / E-mail: miguel.monclus@imdea.org, TEL: +34-91-549-3422, FAX: +34-91-550-3041

KEYWORDS: Al and SiC hardness and modulus, AFM imaging of indenters, High temperature indentation, Indenter area function, Tip degradation

This paper focuses on tip shape and degradation of diamond indenters upon high temperature nanoindentation tests. Accurate indenter area functions (IAFs) are essential for the correct measurement of mechanical properties by instrumented indentation techniques (IIT), particularly during high temperature (HT) nanoindentation. However, being a relatively new technique, sufficient information is lacking. This paper examines the shape and degradation of a Berkovich indenter tip after HT nanoindentation testing of 1 mm-thick SiC and Al thin films at room temperature and at T=100ºC, 200ºC and 300ºC. IAFs were determined by the reference method and by atomic force microscopy (AFM), with the latter giving higher contact areas, although tip defect values extracted from both methods were in good agreement. Examination of the tip by AFM after HT nanoindentation on SiC reveals a blunt tip and the need for a new IAF. The work emphasizes the importance of carrying out indenter tip shape calibrations on a regular basis, especially when indenting and scanning hard samples and metals that readily oxidise at T>200ºC, where the tip gets easily contaminated.

Manuscript received: January 2, 2014 / Revised: March 14, 2014 / Accepted: March 27, 2014

1. Introduction

Interest in hot micro and nano-mechanics has grown in the last few years as the characterization of the mechanical response of small material volumes and thin films at high temperatures is crucial to many new technological applications.[1,2] The instrumented indentation technique (IIT) is the most widely used by researchers worldwide, since there are now well-established methods and standards for the application of nanoindentation to many material types.[3,4] Hot research topics include studies on the effect of elevated temperature on incipient plasticity[5,6] indentation size effect,[7,8] nanoscale multilayers[9,10] and phase transformation.[11] However, high temperature (HT) IIT is still in the early stages of development, as it must overcome many technical challenges such as the control of thermal drift and the thermal stability of both tip and sample surface at the testing conditions (i.e., oxidation and/or chemical reactions between sample and tip). New machine designs, testing environments and protocols are currently being developed to tackle these issues.

This work is motivated by the increasing demand for high temperature indentation characterization and the need to understand how the indenter tip shape affects the measurement of mechanical properties at high temperatures. All nanoindentation based measurements require knowledge of the contact area between the diamond indenter and the test piece and the estimation of the contact area from the load-displacement curve represents the biggest source of errors in nanoindentation measurements, especially for small indentation depths (< 1 mm). The Berkovich diamond indenter (three-sided pyramid), is the most widely used geometry for extracting modulus and hardness values of thin films and small volumes.[12] The contact area between the indenter and the sample can be determined from the contact depth and the calibrated indenter geometry, typically referred to as the indenter area function (IAF). In order to determine the IAF, two methods can be adopted: (i) an indirect calibration, by indenting a reference material exhibiting known elastic properties (e.g., fused quartz) and (ii) a direct measurement of tip area by metrological atomic force microscopy (AFM) of the tip, which is the recommended direct method of obtaining the IAF by the ASTM E2546-07 (ASTM, 2007) and the ISO 14577-4 standards.

In this study, a brand new Berkovich indenter is used to indent SiC and Al 1 mm-thick coatings. The tests were performed from ambient temperatures up to 300ºC. IAFs of the indenter tip were obtained by the reference method performing indentations on a fused quartz sample and by AFM direct imaging before and "in between" the SiC and Al tests, and then used to calculate modulus and hardness values as a function

of temperature using the Oliver and Pharr method[13] and AFM imaging of residual impressions. The tip defect was also examined by direct (AFM imaging) and indirect (from indentions on fused quartz) methods, with good agreement on the calculated tip defect values from both methods. Results demonstrate the importance of monitoring the tip shape during high temperature indentation, as tip wear and contamination from chemical reactions can degrade tips very fast, when indenting metals and ceramics, even at relatively moderate temperatures.

2. Materials and Experimental Techniques

The investigated SiC and Al coatings were grown on single-crystal (100) Si substrates, by physical vapour deposition (PVD) to a thickness of ≈ 1 mm. The Al coating displayed a columnar nanograin structure with a preferred (111) crystalline orientation, while the SiC coatings were amorphous. Samples were cut in 1×1 cm^2 pieces for testing at different temperatures.

Room temperature (RT) and high temperature (HT) nanoindentation measurements were performed using a Hysitron TI950 triboindenter instrument equipped with a hot stage and a Berkovich tip attached to a Zerodur® glass ceramic shaft with negligible coefficient of thermal expansion. Indentation tests were carried out using fast loading cycles in order to minimize thermal drift effects on load-displacement curves. Loading rates of 5 mN/s were used with a hold period of 0.5 s at a maximum load of 10 mN and unloading times of 0.5 s. For Al tests, loads of 2.5, 5, 7.5 and 10 mN were used in order to get a better estimation of the coating-only hardness and modulus by extracting the substrate contribution using the extrapolation method described in ISO 14577 part 4. The extrapolation was done in the range $0.2 < h_c/t_c < 0.5$, where h_c is the contact depth and t_c is the film thickness. The range was chosen in order to minimize roughness effects of the Al films (R_a=13±1 nm) as the ISO standard recommends $h_c > 20R_a$, which corresponds to $h_c/t_c > 0.24$. As a result of this large h_c/t_c ratio, some substrate contributions cannot be ruled out, especially in the determination of modulus. At least 10 indents were performed at each temperature and maximum load, and the samples were kept at the test temperature for at least 3 hours. Samples were mounted with mechanical clips and heated to the selected temperature; once at thermal equilibrium, the tip was brought into contact with the sample surface and allowed to equilibrate for up to 1 hour before performing the tests. A water cooled thermal shield was placed between the loading head and the hot stage to insulate the transducer from direct radiant heat. In order to minimise surface oxide formation, a constant small flow of high purity Ar was maintained near the tip for the full duration of the tests. A Parks XE-150 AFM instrument was used in contact mode to scan the indenter tip and the residual impressions after indentation. The indenter area function was determined only at room temperature as the diamond indenter geometry is not expected to change significantly since diamond thermal expansion coefficient is only 0.8×10^{-6}/K and the diamond tip dilation is less than 0.04% at 400°C.[14]

2.1 Indenter area function (IAF) calculation by reference material

To determine the IAF by a reference material, a series of indentations were performed in a fused quartz sample of known elastic modulus (69.6 GPa) and Poisson´s ratio (0.16). Indentation runs were conducted up to the maximum load for the transducer (12 mN) at various contact depths using constant loading rates, with 5 s loading and unloading times and 2 s hold period. The maximum contact depth was ≈ 200 nm. These same indentations were used for estimating the tip defect which was then compared with AFM 3D profiles. The IAF is obtained from a plot of the calculated contact area (A_c) versus contact depth (h_c) by fitting the curve to the Oliver and Pharr formulation of the form:

$$A_c = C_0h_c^2 + C_1h_c + C_2h_c^{1/2} + C_3h_c^{1/4} + C_4h_c^{1/8} + C_5h_c^{1/16}\ldots \quad (1)$$

where C_0 to C_5 are fitting coefficients.

2.2 Diamond area function (IAF) calculation by AFM imaging

Cleanliness of the tip is crucial to obtain good quality images for IAF calculation. Before AFM scanning, the indenter tip was cleaned with a cotton wool swab soaked with alcohol and dried touching the tip 2~3 times with a clean lens tissue, until no visible contamination was observed under an optical microscope (with a magnification of at least ×200). Occasionally, in order to remove stubborn contamination, low forces were used to push a flat wooden stick (soaked with alcohol beforehand) onto the indenter. The tip was mounted on the AFM base plate by placing it inside a hole of a small Al cylinder, and fixed by means of plasticine. AFM scans were obtained in contact mode using standard Si probes with a very low spring constant (0.2 nm/mN).

The AFM tip was checked and its radius measured before and after indenter scans with an ultra-sharp array of peaks (TipCheck, Aurora Nanodevices Inc.) and the SPIP software equipped with the "tip characterization" tool. An estimated tip radius of ≈ 20 nm ± 2 nm was found before and after tests. Tip dilation effect, which will produce a small overestimation of the contact area, was not considered here, as the sizes of the AFM tip relative to those of the indentation probes (110~445 nm) were small, and the area values between original and re-constructed images are less than 3%. Thus, only data from the original AFM images are reported here.

Visual alignment of the indenter was done using the motorised AFM X-Y stage and the AFM optics. Fine positioning is completed by electronically adjusting the AFM scan window. During imaging, the indenter tip apex was first found by taking a large scan size (i.e. 60×60 mm^2) at low resolution and then progressively zooming in on the tip apex. Final target conditions were scan size of 2×2 μm^2 with 512 pixels/line and a scan rate of 1 Hz with both gain and force optimised as appropriate. The AFM images were then analysed by SPIPTM data processing software (Image Metrology). As the vertical axis of the indenter in the metal holder is not perfectly aligned, the obtained images were tilted to get the indenter axis parallel to the z axis. This was achieved by assuming that the facet angles are equal on both sides of the indenter tip. Line cross sections were obtained through the top of the indenter tip, and then an interactive tilt plane correction was applied until facets at both sides were equal. Datasets of cross-sectional areas orthogonal to the pyramid axis (i.e. projected areas) at different heights were then obtained with an accuracy step of at least 5 nm. The IAF was finally derived from a polynomial fit to the area vs. height data.

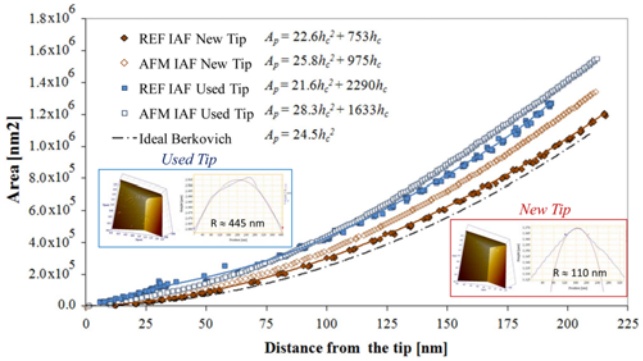

Fig. 1 Indenter area functions (IAFs) measured by AFM and the Reference method of a new tip (diamond symbols) and a used tip (square symbols) with the measured radius of 110 nm and 445 nm respectively, which were obtained from AFM 3D profiles shown in the figure insets. The ideal Berkovich IAF is also shown for comparison

3. Results and Discussion

3.1 Indenter tip characterization

Fig. 1 shows a comparison of the IAFs obtained for the indenter tip (new and then used for HT testing of the SiC layers) and the IAF for an ideal Berkovich indenter. The data for the area obtained with both methods was fitted using two coefficients of polynomial (1). For an ideal Berkovich, A_c=24.5h_c^2. The area calculated from the ideal Berkovich geometry is always smaller than the others due to the bluntness of the tip, which increases the projected area. In general, AFM IAFs are larger than those obtained by reference IAFs,[15] however for low contact depths (h_c<80 nm for used tip and h_c<20 nm for new tip), the area achieved by the AFM IAF is larger than the REF IAF due to tip deformation during indirect determination of IAF using a reference sample.

In practice, new indenters are not perfectly sharp but have a tip radius in the range of 100~200 nm. In Fig. 1, measured tip radii of 110 nm and 445 nm were obtained for the new tip and the same tip after use. This becomes increasingly important as the depth of penetration decreases (low h_c), where the radius of curvature becomes the dominating effect in the IAF.

The tip rounding effect causing a deviation from an ideal tip shape can also be approached by defining a tip defect value "Δh". If Δh represents the "missing portion" from the ideal tip, the penetration depth quantities will be in error by this amount, and the actual contact area at the measured value of contact depth h_c would be:

$$A_c = 24.5(h_c + \Delta h)^2 \tag{2}$$

If the face angles were ideal, then we could find the actual area of contact using (2). The value of Δh can be estimated in two indirect ways:

i) From a contact stiffness (S) versus h_c plot. The contact stiffness for a Berkovich indenter can be expressed as:

$$S = \frac{dF}{dh} = \left(\frac{2}{\sqrt{\pi}}\right) E^* \sqrt{24.5}(h_c + \Delta h) \tag{3}$$

For indentation in a material having constant elastic modulus, such as fused quartz, the relationship between S and h_c is a linear function, and a plot of S versus h_c yields a straight line of the form:

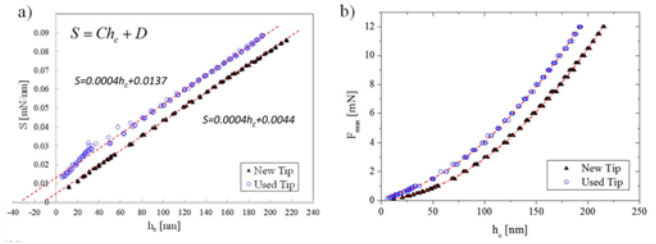

Fig. 2 (a) Curves of stiffness S versus contact depth h_c and linear approximation using Eq. (4); (b) Curves of peak force F_{max} versus contact depth h_c and curve fit using expression (5). All curves determined experimentally on fused quartz with the new (triangles) and the used (open circles) indenter tip

$$S = Ch_c + D \tag{4}$$

The value of Δh is thus found from the intercept term D/C, as shown in Fig. 2(a), by extrapolating the linear part of the curve to zero value of S.

ii) From a maximum force (F_{max}) versus h_c plot. Using the definition of hardness, this curve is given by

$$F_{max} = C_d(h_c + \Delta h)^2 \tag{5}$$

where C_d is the loading curvature and Δh is the blunting distance, which can be approximated as the tip defect. Fig. 2(b) shows the fit to the data obtained in fused quartz. The "Δh" tip defect values calculated from both methods are given in Table 1.

To account for variations in the facet angle [factor 24.5 in Eq. (2)], the area of contact can be calculated from:[16]

$$A = [(\sqrt{\pi}C)/(2\beta E^*)]^2 (h_c + \Delta h)^2 \tag{6}$$

where C is determined from the fitted data (Fig. 2(a)), E^* is the known modulus of the fused quartz and b is a geometrical shape factor with a value of ~1.034 for a Berkovich indenter.

As mentioned, AFM imaging method can be applied to obtain the IAF and to examine other indenter tip features, like defects. Plane-view AFM observations (scan size of 2×2 μm^2) of the new and used indenter tip are shown in Figs. 3(a) and 3(b) respectively. The contour lines are set every 60 nm; the bluntness of the tip centre is more evident in the used indenter tip, which was blunted after indenting and scanning SiC at high temperatures. Tip defect "Δh" can be estimated by extracting and extrapolating lines following the diagonal of the three sided indenter, as shown in Fig. 3. Using this methodology, "Δh" was measured as ~6 nm for the new tip and ~29 nm for the used one. These values are coherent with those obtained by indirect methods (see Table 1). Such an agreement was also found by Krier et al.[17] when using fused silica for the indirect method.

3.2 High temperature indentation testing of SiC and Al thin films

Indentation hardness is defined as the ratio between the maximum

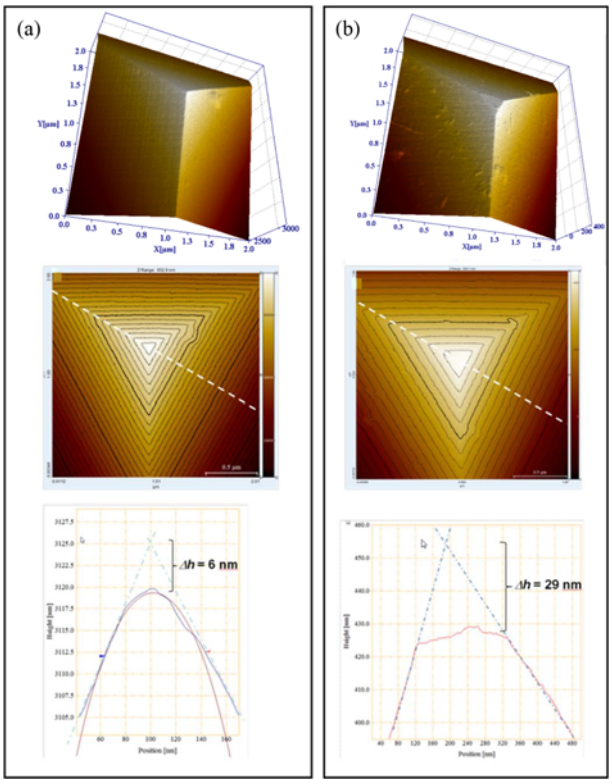

Fig. 3 3D AFM topography, 2D AFM scan image (2×2 μm^2 scan size) with contour lines and cross section along the indenter diagonal from which the tip defect Δh can be estimated for: (a) new tip and (b) used tip after HT testing of SiC

Table 1 Values of tip defect Δh deduced from indirect methods i) contact stiffness (S) versus h_c plot, ii) maximum force (F_{max}) versus h_c plot and from direct observation of the indenter tip by AFM

Δh [nm]	S vs. h_c	F vs. h_c	AFM
New tip	11	11	6
Used tip	34	29	29

applied force (F_{max}) and the projected area of indentation impression (A_p). The Oliver and Pharr allow indirect measurement of A_p through the IAF, which needs to be estimated as accurately as possible. The main limitation of this method is that it cannot account for pile-up around the indenter which happens when indenting soft materials, leading to an underestimation of the contact area and therefore to an overestimation of the measured hardness.[18] Fig. 4 shows two indentation impressions on SiC (a) and Al (b) at T=200°C for the same maximum load of 10 mN. The pile-up behaviour is clearly visible in the case of the Al residual indent; the maximum indentation depth was ≈ 500 nm for Al and ≈ 60 nm for SiC. Hardness was then evaluated by a direct method, imaging the indentation's impression by AFM, which permits direct measurement of the actual area of the indentation impression and the examination of pile-up behaviour, from AFM scans like the one shown in Fig. 5.

In the SiC scan image of Fig. 4(b), pre-indentation scan lines can be observed, as the indenter tip was used for imaging the surface prior to indentation with a setpoint force of 2 mN. It is believed that the tip suffered acute blunting after the HT indentation and scanning on the

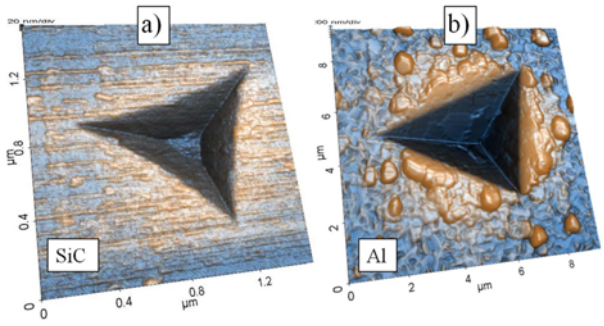

Fig. 4 (a) AFM 3D topography scans of residual indent impressions performed at T=200°C on SiC (a) and Al (b) at a maximum load of 10 mN. Scan sizes are 1.5×1.5 μm^2 and 10×10 μm^2 respectively

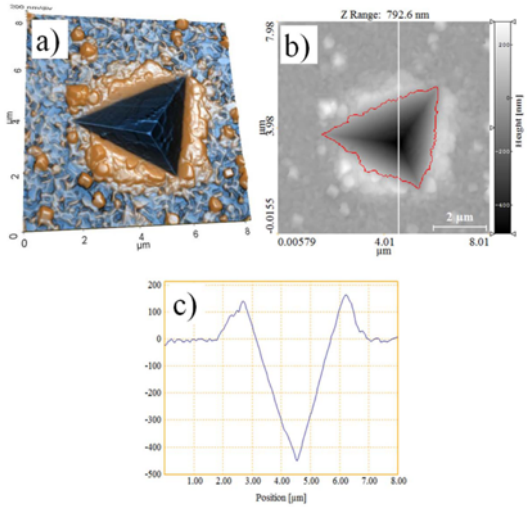

Fig. 5 (a) 3D topography of residual indent on Al (8×8 μm^2 scan size), (b) measurement of projected area (red contour) taking pile-up into account and (c) cross-section across residual indent showing pile-up behaviour

SiC single layers. The combination of applied stress and propensity of diamond reaction with carbide containing materials at elevated temperatures can cause gradual wear of the tip.[12] AFM scans of the tip in Fig. 3(b) and 6(a) confirms the blunting of the tip that occurred after the SiC HT testing.

This blunted tip, which has been called "used tip" throughout this work, was then employed for the Al HT testing. Figs. 6(b) and 6(c) show the residual impressions left on the Al surface at T=200°C and 300°C for a maximum load of 1 mN. The images illustrate how, at T=200°C, the residual impression on the Al surface matches very well the shape of the indenter tip, while at T=300°C, the impression has an irregular shape indicating a high degree of tip shape degradation or contamination. In ambient air or in an uncontrolled atmosphere like the one in which the HT tests took place, oxidation (and erosion) of the diamond indenter is only expected to occur for temperatures ≥ 450°C.[19] Therefore, the rough and uneven imprint observed in Fig. 6(c) was very likely caused by surface oxide contamination attached to the indenter tip during Al HT testing at 300°C. This was then confirmed by the tip scan after the test shown in Fig. 7(b) which reveals the presence of severe oxide

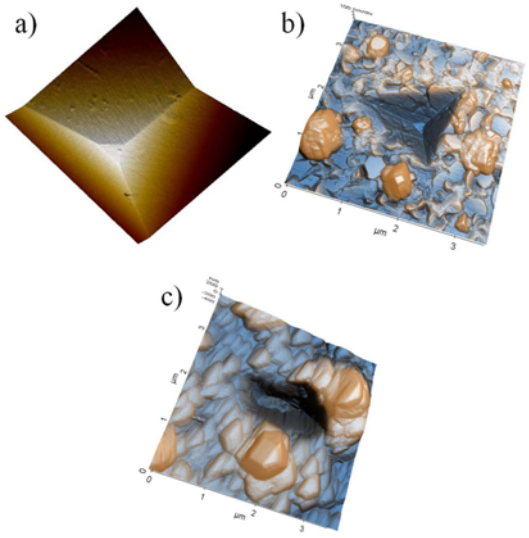

Fig. 6 (a) AFM 3D topography images of blunt tip (2×2 μm^2 scan size), and indent impression on Al surface at (b) T=200°C and c) T= 300°C (3.5×3.5 μm^2 scan size)

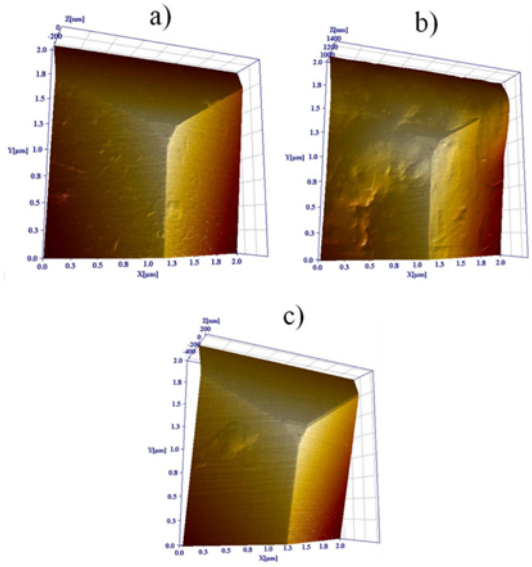

Fig. 7 AFM 3D topography images (2×2 μm^2 scan size) of the blunted tip used to indent Al, (a) before testing, (b) after indenting Al at T= 300°C and (c) after acid treatment on the indenter to remove oxide contamination

contamination strongly adhered around the tip apex. This oxide contamination causes the IAF calculated for the tip useless. In order to remove the oxide contamination, cleaning steps with increased severity were tried, ranging from using solvents and scotch tape to indenting wood and Si. In the end, we found an optimal method, which consisted in applying hot phosphoric acid to the tip in small drops using a cocktail stick, being careful not to attack the diamond holder, and leaving it for a few seconds to act; this was followed by indenting on wood and washing with solvent. This cleaning procedure was repeated several times until most of the oxide was removed, as seen in Fig. 7(c).

Indentation modulus and hardness values for the SiC and Al as a function of temperature are given in Figs. 8(a) to 8(c). Error bars on the graphs represent the standard deviation of 10 indents. Hardness values were obtained from the standard definition using the areas obtained from the reference (REF) and AFM IAFs of the indenter and from direct imaging of residual impressions (AFM analysis). Taking the AFM analysis values, SiC hardness decreases gradually from a RT value of ≈ 35 GPa down to ≈ 29 GPa for T=300°C, whereas the Al hardness decreases from ≈0.9 GPa at RT down to ≈0.4 GPa at T=200°C. These values agree well with those obtained using the REF and AFM IAFs for Al, whereas in the case of SiC, the AFM IAF appears to slightly underestimate the hardness values.

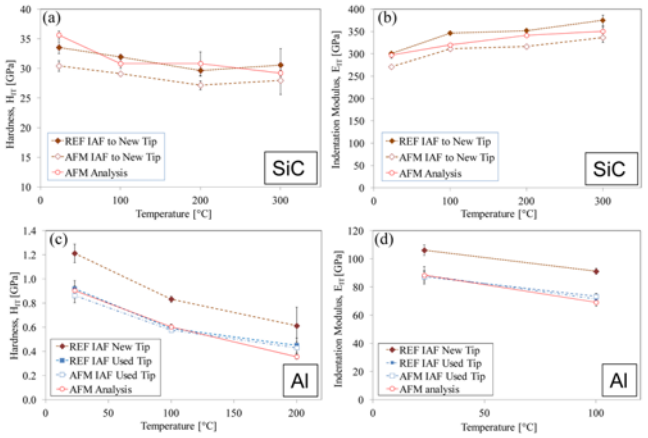

Fig. 8 Indentation modulus (E_{IT}) and hardness (H_{IT}) for SiC (a), (b) and Al (c), (d) single layers as a function of temperature, calculated using the Oliver and Pharr method and contact areas from REF and AFM IAFs and from direct AFM imaging of residual impressions

Indentation modulus were calculated using the standard Oliver and Pharr method using areas evaluated from the REF and AFM IAFs and the area measured directly from AFM imaging, and assuming Poisson ratios of 0.14 and 0.334 for the SiC and Al layers respectively. The trend of the SiC modulus values with temperature is opposite to that of the hardness, with an increase in values from ≈300 GPa at RT up to ≈360 GPa at T=300°C. Normally a small decrease of elastic modulus for SiC as a function of temperature would be expected, which is not seen in this case, probably due to film densification.[20] As observed for the hardness values, the AFM IAF underestimates the modulus values. This is probably due, to the AFM IAF overestimation of the contact area for the new tip at the relevant contact depths, effect that is alleviated for the Al as in this case, the hardness and modulus values were obtained by extrapolating to zero contact depth and size.

For the Al modulus, only the values up to 100°C are shown, since the thermal drift for T=200°C was too large to obtain meaningful results. The Al modulus value decreases from ≈90 GPa at RT down to ≈70 GPa at T=100°C. Results are somewhat larger than expected for Al (E≈72 GPa at RT), but substrate effects cannot be ruled out, because as explained in the experimental section, the lowest indentation depth was set to h_c/t_c=0.2 to minimize surface roughness effects. In the case of Al, the values obtained with the REF and AFM IAFs agree quite well with the AFM analysis. For illustration, in the Al graphs, the values that would be obtained using the IAF for the new tip are also plotted, in order to show how the results that would be obtained are erroneous

since the IAF for the new tip, which was valid for the SiC tests, is no longer valid for the evaluation of the modulus and hardness of Al. The valid IAF in this case is the one corresponding for the used tip - as we know the tip was blunted after the SiC testing.

4. Conclusions

Hardness and modulus values of SiC and Al single layers were measured as a function of temperature. Results using Oliver and Pharr method and AFM imaging of residual impressions agree well, and show the importance of using the right indenter area function for mechanical property measurement, especially since degradation and contamination of the tip can occur fast when indenting metals and ceramics at relatively moderate temperatures.

In this sense, AFM is a very powerful tool for the nanoindentation community as it can be used to obtain indenter area functions in a direct way and also to check tip shape when degradation and / or contamination are suspected. Tip defects can also be attained by AFM, and obtained results showed that they compare very well with indirect methods using indentation curves on a reference sample. AFM scanning of the tip proved quite useful for checking tip bluntness and oxide contamination. The tip shape effect in the determination of hardness and modulus values is particularly relevant for high temperature indentation, especially when indenting hard samples where scanning at elevated temperatures should be minimised in order to avoid rapid blunting of the tip. In addition, when indenting metals like Al that readily oxidised, the tip can get easily contaminated by oxide, and scanning should be minimised, especially in an uncontrolled atmosphere. Hardness can be obtained in a direct way by measuring the real area of indentation impressions by AFM high-resolution imaging in order to take pile-up into account.

ACKNOWLEDGEMENT

The authors gratefully acknowledge financial support from the Spanish Ministry of Economy through grant MAT2012-31889 and though PCIN-2013-029, in the framework of the Materials World Network of the National Science Foundation and professor Nikhilesh Chawla for fabricating the Al and SiC coatings.

REFERENCES

1. Wood, A. J. and Clyne, T. W., "Measurement and Modelling of the Nanoindentation Response of Shape Memory Alloys," Acta Materialia, Vol. 54, No. 20, pp. 5607-5615, 2006.
2. Chen, J., Beake, B. D., Dong, H., and Bell, G. A., "Environmental Nanomechanical Testing of Polymers and Nanocomposites," Nanomechanical Analysis of High Performance Materials, pp.63-84, 2014.
3. Lucca, D. A., Hermann, K., and Klopfstein, M. J., "Nanoindentation: Measuring Methods and Applications," CIRP Annals - Manufacturing Technology, Vol. 59, No. 2, pp. 803-819, 2010.
4. Oliver, W. C. and Pharr, G. M., "Measurement of Hardness and Elastic Modulus by Instrumented Indentation: Advances in Understanding and Refinements to Methodology," Journal of Materials Research, Vol. 19, No. 1, pp. 3-20, 2004.
5. Lund, A. C., Hodge, A. M., and Schuh, C. A., "Incipient Plasticity during Nanoindentation at Elevated Temperatures," Applied Physics Letters, Vol. 85, No. 8, pp. 1362-1364, 2004.
6. Rajulapati, K., Biener, M., Biener, J., and Hodge, A., "Temperature Dependence of the Plastic Flow Behavior of Tantalum," Philosophical Magazine Letters, Vol. 90, No. 1, pp. 35-42, 2010.
7. Franke, O., Trenkle, J. C., and Schuh, C. A., "Temperature Dependence of the Indentation Size Effect," Journal of Materials Research, Vol. 25, No. 7, pp. 1225-1229, 2010.
8. Soler, R., Molina-Aldareguia, J. M., Segurado, J., and LLorca, J., "Effect of Misorientation on the Compression of Highly Anisotropic Single-Crystal Micropillars," Advanced Engineering Materials, Vol. 14, No. 11, pp. 1004-1008, 2012.
9. Monclus, M. A., Zheng, S. J., Mayeur, J. R., Beyerlein, I. J., Mara, N. A., et al., "Optimum High Temperature Strength of Two-Dimensional Nanocomposites," APL Materials, Vol. 1, No. 5, Paper No. 052103, 2013.
10. Lotfian, S., Rodriguez, M., Yazzie, K., Chawla, N., Llorca, J., and Molina-Aldareguia, J., "High Temperature Micropillar Compression of Al/SiC Nanolaminates," Acta Materialia, Vol. 61, No. 12, pp. 4439-4451, 2013.
11. Ruffell, S., Bradby, J. E., Williams, J. S., Munoz-Paniagua, D., Tadayyon, S., et al., "Nanoindentation-Induced Phase Transformations in Silicon at Elevated Temperatures," Nanotechnology, Vol. 20, No. 13, Paper No. 135603, 2009.
12. Wheeler, J. M. and Michler, J., "Indenter Materials for High Temperature Nanoindentation," Review of Scientific Instruments, Vol. 84, No. 10, Paper No. 101301, 2013.
13. Oliver, W. C. and Pharr, G. M., "An Improved Technique for Determining Hardness and Elastic Modulus using Load and Displacement Sensing Indentation Experiments," Journal of Materials Research, Vol. 7, No. 6, pp. 1564-1583, 1992.
14. Schuh, C. A., Packard, C. E., and Lund, A. C., "Nanoindentation and Contact-Mode Imaging at High Temperatures," Journal of Materials Research, Vol. 21, No. 3, pp. 725-736, 2006.
15. Choi, J. H. and Korach, C. S., "Tip Bluntness Transition Measured with Atomic Force Microscopy and the Effect on Hardness Variation with Depth In Silicon Dioxide Nanoindentation," Int. J. Precis. Eng. Manuf., Vol. 12, No. 2, pp. 345-354, 2011.
16. Fischer-Cripps A. C., "Nanoindentation," Springer, pp. 86-87, 2011.
17. Krier, J., Breuils, J., Jacomine, L., and Pelletier, H., "Introduction of the Real Tip Defect of Berkovich Indenter to Reproduce with FEM Nanoindentation Test at Shallow Penetration Depth," Journal of Materials Research, Vol. 27, No. 1, pp. 28-38, 2012.

18. Bull, S., "Nanoindentation of Coatings," Journal of Physics D: Applied Physics, Vol. 38, No. 24, pp. R393-R413, 2005.

19. Wheeler, J., Oliver, R., and Clyne, T., "AFM Observation of Diamond Indenters after Oxidation at Elevated Temperatures," Diamond and Related Materials, Vol. 19, No. 11, pp. 1348-1353, 2010.

20. Snead, L. L., Nozawa, T., Katoh, Y., Byun, T. S., Kondo, S., and Petti, D. A., "Handbook of SiC Properties for Fuel Performance Modeling," Journal of Nuclear Materials, Vol. 371, No. 1, pp. 329-377, 2007.